THE DAVID W. TAYLOR MODEL BASIN

UNITED STATES NAVY

MEASUREMENTS ON SHOCK WAVES IN WATER WITH THE HIGH-SPEED SPARK CAMERA

BY Dr. A. KEIL

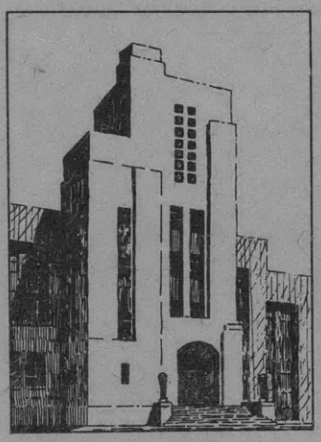

SEPTEMBER 1947

TRANSLATION 213

MEASUREMENTS ON SHOCK WAVES IN WATER WITH THE HIGH-SPEED SPARK CAMERA

(MESSUNGEN AN STOSSWELLEN IN WASSER MIT DER FUNKENZEITLUPE)

by

Dr. A. Keil

Dänisch-Nienhof, July 1946

Translated by R. Widmer

Navy Department
David Taylor Model Basin
Washington, D.C.

September 1947 Translation 213

TABLE OF CONTENTS

MEASUREMENTS ON SHOCK WAVES IN WATER WITH THE HIGH-SPEED SPARK CAMERA

INTRODUCTION

Acoustics deals with periodic phenomena of "infinitely small" amplitude, wherein the pressure variations are slight with respect to the state of rest. Mathematical treatment of these problems is especially simple and culminates in the generally familiar laws, such as, for example, the law of constant velocity of propagation of such waves or the 1/e-law* of the decrease of amplitude of spherical waves with distance.

The behavior of shock waves, wherein aperiodic phenomena of great (finite) amplitude are concerned (a sudden pressure rise, or, in effect a discontinuous pressure rise, followed by a gradual pressure drop), naturally digresses from acoustic laws. In this respect, the most striking feature is the fact that the velocity of a shock wave is a function of its amplitude.

Now, the measurement of pressure fields is a relatively difficult task in acoustics, since in a nonstationary sonic field measurements must be made at a large number of stations simultaneously, or in a stationary sonic field measurements must be made consecutively at the greatest number of points possible with one pickup gage. Although similar difficulties are met in the measurement of the pressure fields of shock waves, which are likewise nonstationary, only shock waves in water will here be treated.

Generally, diaphragm pressure gages are used for measurement of shock waves in water. These are particularly simple mechanical gages which have proved satisfactory in use. Owing to their size, these pressure gages are unsuitable for laboratory tests, and their technical characteristics further make them useless for many systematic investigations (1).**

By use of the high-speed spark camera and because of the functional relationship of the velocity of a shock wave to its amplitude previously indicated, it has been possible to develop a method, which will be here described and whose applicability will be illustrated by several examples. However, before taking up individual factors involved, the principle of high-speed spark cameras must be treated in somewhat greater detail.

THE HIGH-SPEED SPARK CAMERA

The basic concept of the high-speed spark camera can be traced to Carl Cranz and to Hubert Schardin (2), of whom the latter especially made decisive contributions to the development of this apparatus.

---

* In this translation, e is the distance from the center of propagation to the wave front.

** Numbers in parentheses indicate references on page 29 of this translation.

High-speed spark photography is based on the principle that under proper operating conditions it is possible by means of an aperiodic spark to attain a very intense and extremely brief emission of light whose duration is of the order of 10^{-7} second. With such illumination a high-speed photograph of even the most extremely high-speed phenomenon can be recorded. Figure 1 shows the principle of the arrangement. The light produced by a spark is projected into the objective lens of a camera by a large condensing lens about 50 cm in diameter and having a focal length of 3 m. This objective projects a shadow image of an object, situated between the condensing lens and the camera, upon the photographic plate.

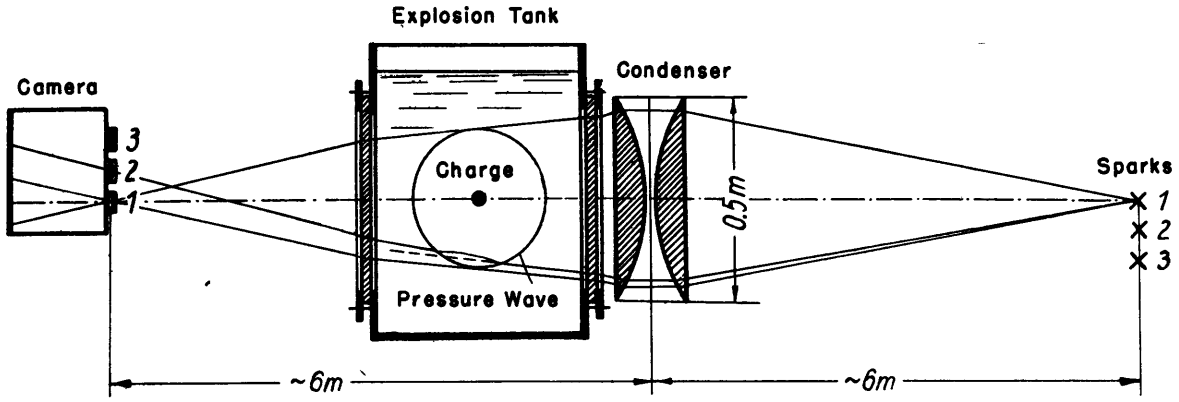

Figure 1 - Test Setup for Photographing an Underwater Explosion with the High-Speed Spark Camera

The attainment of a series of images is achieved by mounting a number of spark gaps as closely beside each other as possible and by using a special camera equipped with as many lenses as there are sparks produced by the spark gaps. If the image of each spark is projected through a condensing lens exactly into an objective it is then necessary only to cause the sparks to jump in close succession at the desired intervals of time. This can be accomplished by using a circuit originated by Mach (2) which is shown in Figure 2. With each spark gap n (n = 1, 2, 3 ...) is associated an electrical oscillatory circuit, consisting of the capacitors C_n and D_n and of high-ohmic resistances R_n and S_n. The individual circuits are connected by one inductance L_n apiece, which produces the time lag of the sparks with respect to each other. A potential of several kilovolts is applied to the whole system. Then the electrodes A are the only electrodes between which there is a difference in potential. If the spark is caused to jump between the electrodes of this trip spark gap (by closing the gap between the electrodes, for example), the capacitor C_1 discharges through A and a voltage

is produced at the electrodes of spark gap 1, which, for a purely periodic discharge at A, would be double its original value. However, owing to the damping which occurs, it does not quite reach this value. If the spark gap is long enough, this surge causes the capacitor D_1 to discharge to C_1, and the first illuminating spark jumps. Here the resistors R_1 and S_1 have the practical effect of insulators, in contrast to conditions when charging is slow. After D_1 has discharged, the capacitor C_2 discharges to D_1 with a time lag governed by L_1, thus causing the second illuminating spark to jump, and so on. The smaller the value of L_n is kept, the shorter the time lag between the successive sparks, and hence the higher the frequency of the images obtained.

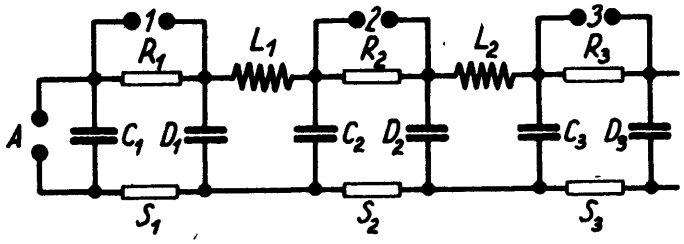

Figure 2 - Schematic Diagram of the High-Speed Spark Camera

In this way, image frequencies ranging from 10^4 to 2×10^6 per second can be attained, which could never be reached in the ordinary manner by recording motion pictures on moving film. A disadvantage, however, is the limited number of images, which naturally is a function of the number of illuminating sparks. Series of 24 images have been found most practical. This is the number used in the high-speed spark cameras designed under the direction of H. Schardin (3). It is highly important for the quality of the images in a series that the sparks be sharply focused and closely spaced, since otherwise the portrayal of the progress of a phenomenon may be adversely affected by parallax.

As an example, the photographic recording of the propagation in water of two shock waves of differing intensity is shown in Figure 3. The sequence of exposures is indicated by the legends given on the pictures. The actual shock waves are made visible by the schlieren effect; see individual pictures Numbers 1 through 19 of Figure 3. It can be noted in the first frames in this figure - even without plotting - that the more intensive shock wave, visible at the center of the photograph, is propagating at a considerably higher velocity than is the very weak spherical wave, seen in the upper portion of the image field. The nonuniform brightness of the image field,

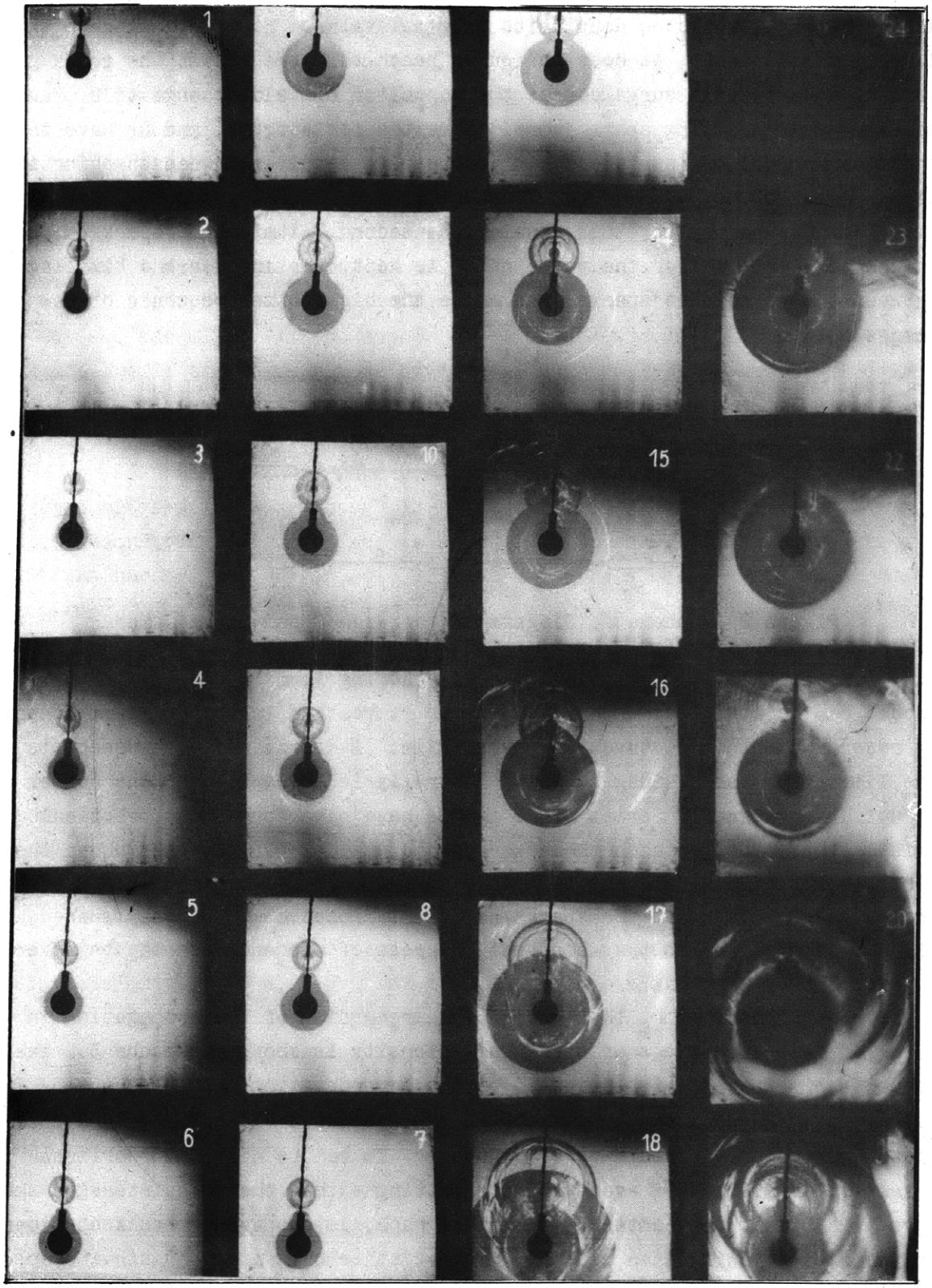

Figure 3 - Example of a High-Speed Spark Photograph
(Propagation of the Spherical Shock Wave)

observable in a number of the exposures, can be traced in some instances to a nonuniform illumination of the condensing lens.

As the photographic recording just discussed shows, the particular value of high-speed spark photography is due to the almost automatic schlieren effect, produced by the experimental apparatus itself, which makes all variations in density, and hence particularly pressure waves, visible. The variations in density occurring in the pressure wave produce variations in the index of refraction and thus cause a deflection of the light rays from their normal path. A ray of light emanating from illuminating spark 1, which would normally have entered objective lens 1, is refracted toward the center by the pressure wave which operates as a lens. Therefore, it is impossible for this ray to enter objective lens 1, but possibly it may enter one of the other objectives. Consequently the wave front, in which refraction is most intense in shock waves, appears dark in Frame 1, whereas in one of the other frames the refracted light becomes noticeable as a bright crescent.

This peculiarity of the method of recording by high-speed camera signifies a sharp extension of the range of application of high-speed spark photography. The quality of schlieren photographs can be improved still further by use of a special schlieren stop. This consists basically of a knife edge, mounted in front of each objective, which blocks half the image of the linear spark, projected by the condensing lens (3). The quality of schlieren images can be further improved if the individual sparks are not permitted to jump freely in air, but inside slender glass tubes slipped over the tips of the electrodes. This artifice not only results in a more brilliant spark, but above all it fixes the path of the spark, which is important for a sharp definition of the spark at the edges of the schlieren stops.

The special high-speed spark camera with which the tests herein described were made was developed and built in the Ballistic Institute, under the direction of Dr. Hubert Schardin. A detailed description of its structure and design would exceed the scope of this study and will therefore be omitted.

With respect to experimental technique, it should be added that the intense shock waves in water are produced by detonating small amounts of explosive. However, after some experience and by observing the requisite safety measures, the difficulties thus arising can be overcome. In particular, experimental control of the testing area was achieved by using a large explosion tank, 2.5 m in diameter, in which the explosives were detonated. However, the necessity of projecting the beam of light through a column of water of the same diameter as that of the tank occasioned such a loss in light intensity that it was scarcely possible to get usable photographs. Therefore,

successful tests were impossible until a small supplementary condensing lens was mounted in the path of the beam projected from each of the 24 spark gaps. Since the useful light flux from the usual apparatus shown in Figure 1 amounts to only about 1:15 to 1:20, owing to the distance of 6 m from the condensing lens, it is immediately comprehensible that the brightness of the image field could easily be increased by at least a factor of 10 by use of the supplementary condensing lenses.

The necessity for using such high image frequencies as are attainable with high-speed spark cameras probably requires some additional explanation. The usual image field of the apparatus, which is at most 40 cm in diameter, is traversed by a normal sound wave in water produced at the center of the image field in slightly more than 10^{-4} second. As 24 exposures are available in each series of spark photographs, a uniform recording of even this phenomenon requires a frequency exceeding 10^5 cycles per second. However, the velocity of very intense shock waves is considerably higher than the velocity of sound in water, so that even higher frequencies can usually be employed successfully. Since the velocity of such shock waves changes during their propagation (for spherical waves it decreases rapidly with distance), it is advisable to vary the frequency of exposures in each series, i.e., to use the highest frequencies in the zones of most rapid propagation for the best resolving power, and to use lower frequencies as the speed of the phenomenon decreases.

In the tests described in the following pages, this method was successful, but only because it was possible to fix the time of radiation of the shock waves precisely within several 10^{-7} second and to start the recording of the succession of images with corresponding exactitude.

EVALUATION

A number of difficilties are encountered in plotting a series of images obtained with a high-speed spark camera. A primary source of disturbance is that the time lapse between the individual illuminating sparks cannot be reproduced exactly. It is determined by the value of the self-inductance L, as seen in Figure 2. However, the uncontrollable ignition lag of the sparks intervenes, which remains disturbingly evident despite the preionization of the spark gaps which was done with this high-speed spark camera. For this reason also, the frequency of images in a series is not uniform. The scattering of the intervals between the illuminating sparks with respect to each other becomes increasingly evident as the frequency rises and produces deviations of 50 per cent and more from 1 to 2×10^6 cycles per second.

As the problem of interest here deals with the exploitation of a relationship between the velocity of a shock wave and its amplitude, velocities must be measured with the greatest possible precision. However, for this purpose, a knowledge of the individual intervals of time from one spark to the next is absolutely necessary, and such measurements of extremely short lapses of time, which must be made simultaneously with the photographic recording, always present considerable difficulties. In investigating the problems which are to be described in this treatise, these difficulties can be obviated in a simple way. If a shock wave is produced in water, say by an underwater spark or a small detonator,* it propagates with the velocity of sound. Experimentally, this can be proved directly by producing two such pressure waves in quick succession and photographing both simultaneously. Then, if the diameter of the first wave is plotted as a function of the diameter of the second, a linear curve with a slope of 45 degrees is obtained. From this it is immediately evident that both waves propagate at sonic velocity, for if the amplitude of the waves were so high that notable digressions from the velocity of sound occurred, the wave produced later would necessarily have the greater amplitude and hence the greater velocity, which would be shown by a different slope of the curve giving the diameter of one as a function of the other.

By placing a scale in the image field and photographing it also, each photograph is supplied with a linear scale in addition to the time base. Thus the basic requirements for plotting are assured.

As mentioned at the beginning, the parallax which is produced by the spatial disposition of the illuminating sparks may constitute a disturbing factor. Owing to the distance at which the pictures are recorded, i.e., at 6 m as shown in Figure 1, and the successful mounting of the 24 spark gaps within a space of 15 × 20 cm, this disturbance remains so slight that it can be neglected.

Evaluation can be effected most accurately if the photographs are measured directly with a measuring microscope. However, this is very clumsy and is only applicable for analysis of special aspects of the phenomena. Yet the exactitude of the results obtained often justifies the extra expenditure of effort.

Simpler and capable of much broader anaylsis are the vivid propagation charts, such as that shown in Figure 7. They are obtained by projecting the individual frames of a series in consecutive order, on the same place on a drafting board, and sketching the contours. It is better, however, to

---

* A detonator consists basically of a hot wire surrounded by approximately 20 mg of detonating charge (usually lead azide).

make the largest possible reproductions or prints, all enlarged uniformly, of the individual photographs. Then, from these, the wave fronts should be drawn over one another. All the propagation charts included in this study were prepared by the latter method. To increase the precision of plotting, the individual photographs were enlarged 15 times. Since the photographs reproduce the original phenomenon at a 1:5 reduction, the propagation charts show the phenomenon to be investigated from double to triple natural size; see Figures 7 and 8.*

Unfortunately, owing to technical difficulties, all the individual photographs available from a high-speed spark camera recording could not be utilized. In most cases, only every other picture could be used. Naturally, the accuracy of analysis suffers somewhat from this fact.

Even visual examination of a propagation chart discloses the pressure distribution in the shock wave. If two successive wave fronts are traced about the center of impact, a variation of the distances between these curves shows, for example, that the pressure in the front of the shock wave varies. Owing to the greater velocity of propagation, a greater pressure corresponds to the greater distance.

The exact determination of the velocity of shock waves is accomplished, then, as follows. The distances traversed by the shock wave to be measured are plotted as functions of the distances covered by the pressure wave serving as a time calibration. Thereupon, these curves are differentiated graphically. With some practice, evaluation can be made with great accuracy, as was ascertained by comparison of several analyses made independently of each other. The reproducibility of the results obtained will be treated in greater detail in the discussion of the individual problems taken up herein.

VELOCITY OF THE SHOCK WAVE

As already mentioned, the velocity of shock waves is a function of their amplitude. As the velocity of such shock waves can be measured with the high-speed spark camera described in the foregoing, a knowledge of this relationship is necessary. For the case where the amplitudes are not inordinately great, this relationship can be expressed mathematically (4).

If U denotes the energy per unit volume, p the pressure, and v the specific volume of the medium directly behind the front of the pressure wave, and U_0, $p_0 = 1$, and v_0 are used to denote corresponding values in the undisturbed medium ahead of the front of the shock wave, and if a signified the

---

* Editor's Note: The reproductions of these charts which appear in this translation are approximately two-thirds the size of the original charts.

velocity of propagation of the wave, we find according to Hugoniot (5) that

$$a^2 = v_0^2 \frac{p - 1}{v_0 - v} \qquad [1]$$

$$2(U - U_0) = (p + 1)(v_0 - v) \qquad [2]$$

To solve this equation by determination of U, the equation of state of the water must be used. However, Tamman's approximation (6), which is usually used,

$$(v - b)(p + K) = CT \qquad [3]$$

does not satisfy requirements, as the results of the following calculation will show. Since Bridgman's measurements (7) are available as a basis, the calculation was performed with an equation of state which was expressed by a development in a series with respect to the positive pressure variation $\pi = p - 1$ and with respect to the temperature variation $t = T - T_0$, as follows

$$v = v_0(1 + \alpha t - \kappa\pi + \beta\pi t - l\pi^2 + \gamma t^2) \qquad [4]$$

In the foregoing equation, as will be shown later, the term γt^2 can for the present be neglected. The values for the coefficients in the development in a series, Equation [4], are found from the cited measurements by Bridgman to be

$v_0 = 1.00016 \text{ cm}^{-3} \text{ gm}^{-1}$ $\qquad$ $\beta = 8 \times 10^{-8} \text{ atm}^{-1} \text{ degree}^{-1}$

$\kappa = 4.5 \times 10^{-5} \text{ atm}^{-1}$ $\qquad$ $\gamma = 6 \times 10^{-6} \text{ degree}^{-2}$

$l = 1 \times 10^{-8} \text{ atm}^{-2}$ $\qquad$ $c_p = 1 \text{ cal degree}^{-1} \text{ gm}^{-1}$

$\alpha = 2.1 \times 10^{-4} \text{ degree}^{-1}$ $\qquad$ $T_0 = 293^\circ \text{ K} = +20^\circ \text{ C}$

According to thermodynamics it can be stated that

$$dU = -p\,dv - d'q$$

where $d'q = 0$ denotes an adiabatic change of state. Written out, this equation states that

$$dU = \left(-T\frac{\partial v}{\partial T} - p\frac{\partial v}{\partial p}\right)dp + \left(c_p - p\frac{\partial v}{\partial T}\right)dT \qquad [5]$$

and using the equation of state, Equation [4], we then obtain

$$dU = \left[-Tv_0(\alpha + \beta\pi) + v_0(\pi + 1)(\kappa - \beta t + 2l\pi)\right]dp + \left[c_p - v_0(\pi + 1)(\alpha + \beta\pi)\right]dT \qquad [6]$$

where βt can be neglected for the same reason as γt^2 was neglected previously. If we integrate here from U_0 to U_1 while holding p constant, and then from U_1 to U while holding the temperature constant, it is found after combining the results with the equation for energy, Equation [2], and by neglecting higher π-powers, that

$$\frac{\pi}{1 - \frac{v}{v_0}} = \frac{1}{\kappa} \frac{1 + \left(\beta - \frac{\alpha}{2}\right)\frac{v_0}{c_p}\pi}{1 - \frac{\alpha^2 T_0 v_0}{\kappa c_p} + \left[\frac{l}{\kappa} - \frac{3}{2}\frac{\alpha\beta T_0 v_0}{\kappa c_p} + \left(\beta - \frac{\alpha}{2}\right)\frac{v_0}{c_p}\right]\pi} \qquad [7]$$

Since $\frac{\alpha^2 T_0 v_0}{\kappa c_p}$, the constant term appearing in the denominator, is much less than unity as can be recognized by simply substituting the numerical values given previously, it is found that

$$\frac{\pi}{1 - \frac{v}{v_0}} = \frac{1}{\kappa}\left[1 + \frac{\alpha^2 T_0 v_0}{\kappa c_p} + \left(\frac{3}{2}\frac{\alpha\beta T_0 v_0}{\kappa c_p} - \frac{l}{\kappa}\right)\pi\right] \qquad [8]$$

for sufficiently small values of π.

Now, the normal sonic velocity is determined from the adiabatic condition $d'q = 0$ as the velocity of propagation of an adiabatic change of state, which, considering Equations [5] and [4], is written out in full as

$$c_p\, dT = T v_T\, dp = v_0 T(\alpha + \beta\pi)\, d\pi$$

Using the initial condition that the temperature variation t vanishes for $\pi = 0$, integration gives

$$t = T_0\left(C^{\frac{v_0}{c_p}(\alpha + \frac{\beta}{2}\pi)\pi} - 1\right)$$

and from the foregoing by development in a series and by considering Equation [5]

$$v = v_0\left[1 + \pi\left(\frac{v_0 \alpha^2 T_0}{c_p} - \kappa\right) + \cdots\right]$$

Therefore, the adiabatic compressibility is

$$\kappa_{ad} = -\frac{1}{v_0}\left(\frac{\partial v}{\partial \pi}\right)_{ad\,(\pi = 0)} = \kappa\left(1 - \frac{v_0 \alpha^2 T_0}{\kappa c_p}\right) \qquad [9]$$

and the normal velocity of sound is

$$a_0 = \sqrt{\frac{v_0}{\kappa_{ad}}} \qquad [10]$$

After this intermediate calculation, the velocity of the shock wave given by Equation [1] can be expressed in relationship to this sonic velocity as

$$a^2 = v_0 \frac{\pi}{1 - \frac{v}{v_0}} = a_0^2 \kappa \left(1 - \frac{v_0 \alpha^2 T_0}{\kappa c_p}\right) \frac{\pi}{1 - \frac{v}{v_0}}$$

However, from the foregoing and due to Equation [8] and by neglecting $\frac{v_0 \alpha^2 T_0}{\kappa c_p}$ for small π

$$a = a_0 \left[1 + \left(\frac{3}{4} \frac{\alpha \beta T_0 v_0}{\kappa^2 c_p} - \frac{l}{2\kappa^2}\right) \kappa \pi\right] \qquad [11]$$

From the experimental data given previously it follows directly that

$$\frac{3}{4} \frac{\alpha \beta T_0 v_0}{\kappa^2 c_p} \approx 0.05; \quad -\frac{l}{2\kappa^2} = 2.5$$

so that for shock waves in water

$$a = a_0 \left(1 - \frac{1}{4\kappa} \frac{\partial \kappa}{\partial \pi} \pi\right) = a_0 (1 + 2.5 \kappa \pi) \qquad [12]$$

is valid to a close approximation.

In carrying out the calculation γt^2 was neglected in setting up the series [4] for the equation of state. Justification of this procedure is shown in the following: If from Equation [4] in which γt^2 is neglected and from Equation [8], the temperature $t = \frac{\alpha T_0 v_0}{c_p} \pi$ is determined approximately, and if this approximate value is substituted for the temperature in γt^2, the equation of state, Equation [4] neglecting higher powers of π, becomes

$$v = v_0 \left[1 + \alpha t - k\pi + \beta \pi t + \left(-l + \frac{\gamma \alpha^2 T_0^2 v_0^2}{c_p^2}\right) \pi^2\right]$$

Since owing to the experimental data given previously

$$\frac{\gamma \alpha^2 T_0^2 v_0^2}{l c_p^2} \approx 1.5 \times 10^{-3}$$

neglecting γt^2 in Equation [5] is justified.

In general, it is also of interest in this connection to note that, for the effect of the dependence of a shock wave on its amplitude, terms of second order in the equation of state are definitive, as can be seen from Equation [11] and [12]. The effect cannot be expressed, hence, by an equation of state containing three constants, of the type represented by Equation [3].

The calculation made is limited, as an approximation, to small excess pressures π. For more intense shock waves, a simple formulation of the relationship between amplitude and velocity cannot be obtained. However this relationship can be determined if, starting from Bridgman's data (7), an equation of state for water at high pressures is derived. Corresponding calculations by Burkhardt (8), together with the possible small deviations in the shock wave due to possible compressibility of the water (9), give the relationship between the shock wave and its velocity as shown in Figure 4, wherein the velocity is expressed in multiples of the sonic velocity. For small pressure impacts, the curve shown is expressed by Equation [12].

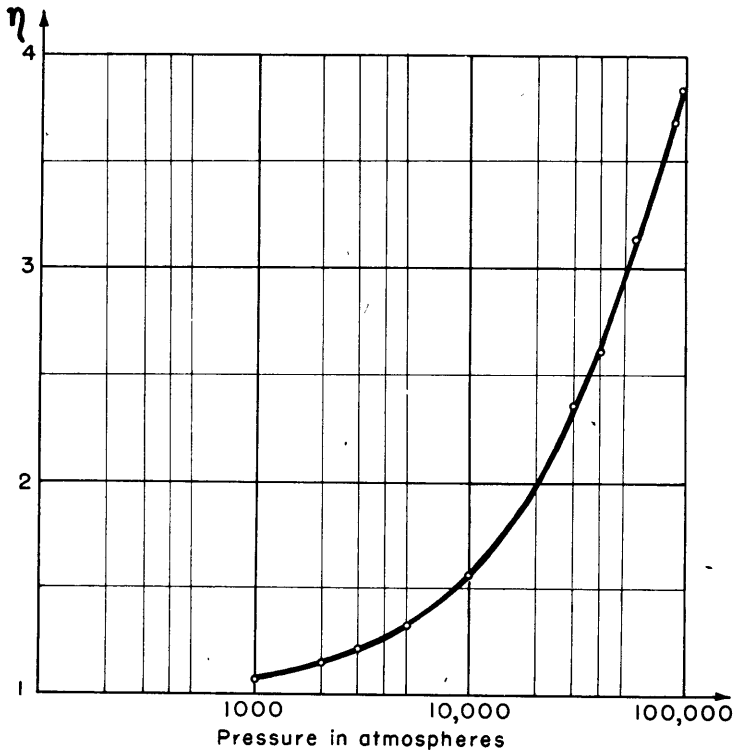

Figure 4 - Velocity of a Plane Compression Shock in Water as a Function of Pressure

The symbol η is the ratio of the shock-wave velocity to the sound velocity.

All the foregoing considerations relate to plane shock waves and cannot, therefore, be adopted directly for waves having curved fronts. However, at large distances of a wave from the center of propagation, the foregoing relationships will be approximately correct and will at least furnish an idea of the order of magnitude of the pressures prevailing there. In any case, it can be assumed with certainty that the curves of equal velocity of propagation determined in a pressure field are also curves of equal pressure.

UNDISTURBED PRESSURE ZONES

For the practical application of the method of pressure measurements described previously, the possibility of reproducing test results is of primary interest. To check the magnitude of the scattering of the measurements, more exhaustive investigations were made on pressure fields produced by spherically symmetrical "shock-wave radiation sources," i.e., spherical explosive charges. Spheres of explosive of diameter r_0 = 1.2 cm were used. These spheres of explosive were cast of a mixture composed of 50 per cent TNT and 50 per cent PETN. The detonator used was inserted into a hole in the charge, so that detonation began practically at the center of the charge.

Figure 3 shows a corresponding high-speed spark camera recording of the phenomenon. The test setup can be recognized on the 24 individual photographs. At the center of the image field, the spherical charge as well as the spherical shock wave shows up dark. In the upper part of the image field, the weak pressure wave used as a time base can be observed. The protuberances at the upper part of the shock wave are pressure waves, which originate at initiation of detonation and which cannot be prevented, but which do not occasion any disturbance. The wires projecting into the image from the top, which bear the charge, serve also as electrical leads supplying the input voltage for firing the charge. By comparing the two gas globes, it can be recognized immediately that, at the beginning particularly, the shock wave produced at the center of the photograph propagates at a considerably greater velocity than does the weaker pressure wave which serves as a time base.

To check the scattering, several photographic recordings of the same type were evaluated as accurately as possible, by determining with a measuring microscope the horizontal diameter of the shock wave and the time-indicating pressure wave in each frame of the series; see Figure 3. Allowing for the small deviations in the focal lengths of the 24 camera objective lenses, and the resultant varying reduction in the image, the distance-time curves for the wave propagation were plotted and graphically differentiated. The principle of this method of evaluation is shown in Figure 5. The velocity ratio is plotted on the basis of the corresponding pressures in Figure 4.

In this way the shock-wave velocities prevailing at various distances from the center of the sphere were obtained. It is simplest to express the distances from the center in multiples of the radius r_0 of the explosive charge and the velocity in multiples η of the sonic velocity. The following table gives a comparison of the values found from a series of such measurements. It shows the relatively great accuracy of the method.

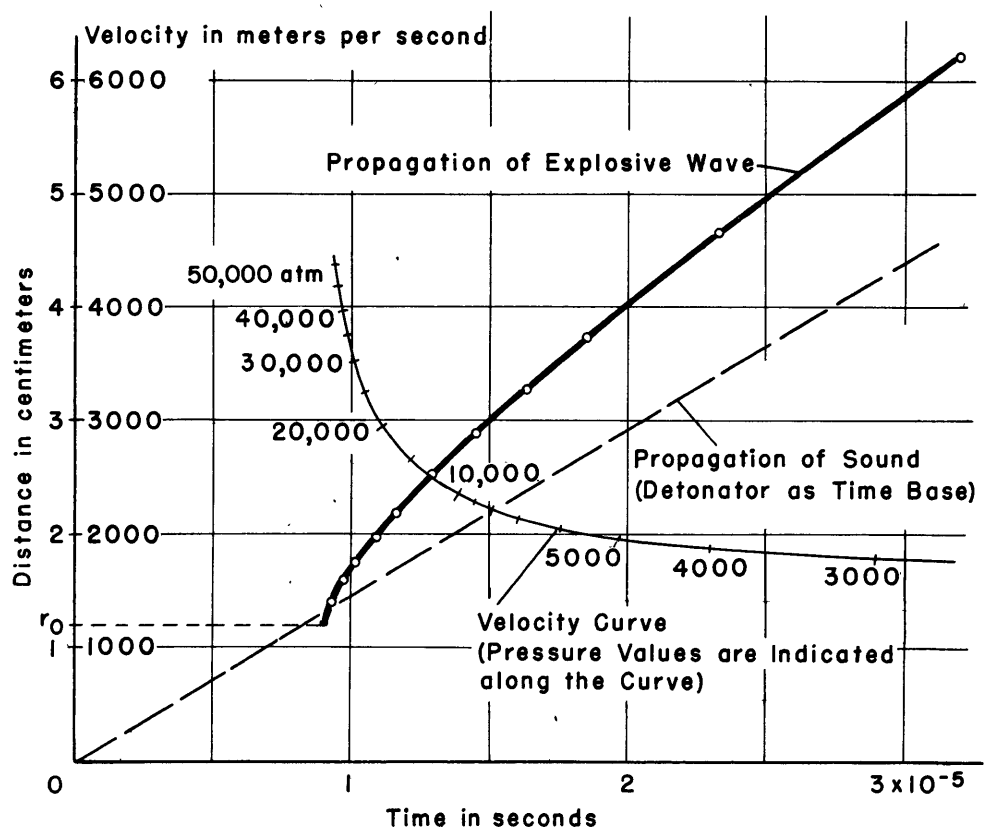

Figure 5 - Evaluation Principle of a High-Speed Spark Camera Photograph (Propagation of a Spherical Shock Wave)

Distance in r_0	$\eta = \frac{\text{Shock-Wave Velocity}}{\text{Velocity of Sound}}$								Mean Value	Pressure in atmospheres
1.5	2.34	2.35	2.35				2.35	2.38	2.35	28,300
2.0	1.82	1.74	1.75			1.70	1.73	1.77	1.75	13,300
2.5	1.54	1.52	1.50	1.50	1.46	1.49	1.48	1.47	1.50	8,200
3.0	1.39	1.40	1.36	1.35	1.33	1.38	1.36	1.34	1.36	5,750
3.5	1.32	1.32	1.30	1.28	1.29	1.32	1.30	1.28	1.30	4,740
4.0	1.27	1.27	1.25	1.25					1.26	4,050
4.5	1.25	1.24	1.21						1.23	3,675

The values appearing in the table show at once that the pressure drop is not in ratio to the reciprocal of the distance, but that the drop is greater. This behavior is even more evident from Figure 6. The measurements plotted in Figure 6, shown by the heavy, solid curve, permit readily inferring a pressure of detonation of approximately 100,000 atmospheres on the

surface of the explosive; compare Figure 7. Initially, the pressure drops very rapidly, and as the distance increases it drops to a level set by the 1/e-law. This is to be expected since as the pressure decreases the laws of acoustics will ultimately apply.

As a confirmation of the practicability of the measuring method as such, the fact must be considered that the pressure drop found here converges toward those values found by measurements made with piezoelectric quartz-crystal gages on shock waves of such type.

Since the practicability of the method here used has been demonstrated, particularly for higher pressures from about 1000 atmospheres upward, the same example, i.e., spherical waves, will be used to carry out a sample analysis of the entire field of the shock wave. For this purpose it is necessary to prepare a wave propagation chart, such as shown in Figure 7. As the velocity of propagation must always be measured perpendicular to the front of the shock wave, the orthogonal trajectories in various directions must be drawn in for the wave fronts indicated by fine lines in Figure 7. Along each of these, the corresponding distance-time curve must be drawn and graphically differentiated. By connecting all those points on the various trajectories where the same shock-wave velocities prevail, the constant-pressure curves are obtained as explained in the foregoing. In Figure 7 they are plotted as heavy, solid curves according to the relationship shown in Figure 4, and the numerical pressure values are included. The curves thus measured show for practical purposes that the shock wave is spherically symmetrical in this instance.

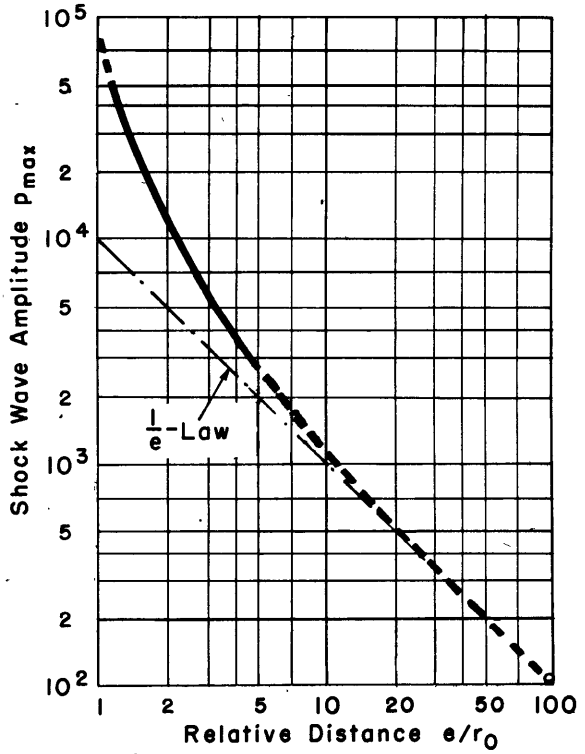

Figure 6 - Decrease of Pressure with Distance for Spherical Shock Wave

As a second example of an undisturbed pressure field, that shown in the wave-propagation chart, Figure 8, may be used. It was recorded from detonation of a "line charge" consisting of 50 per cent TNT and 50 per cent RDX.

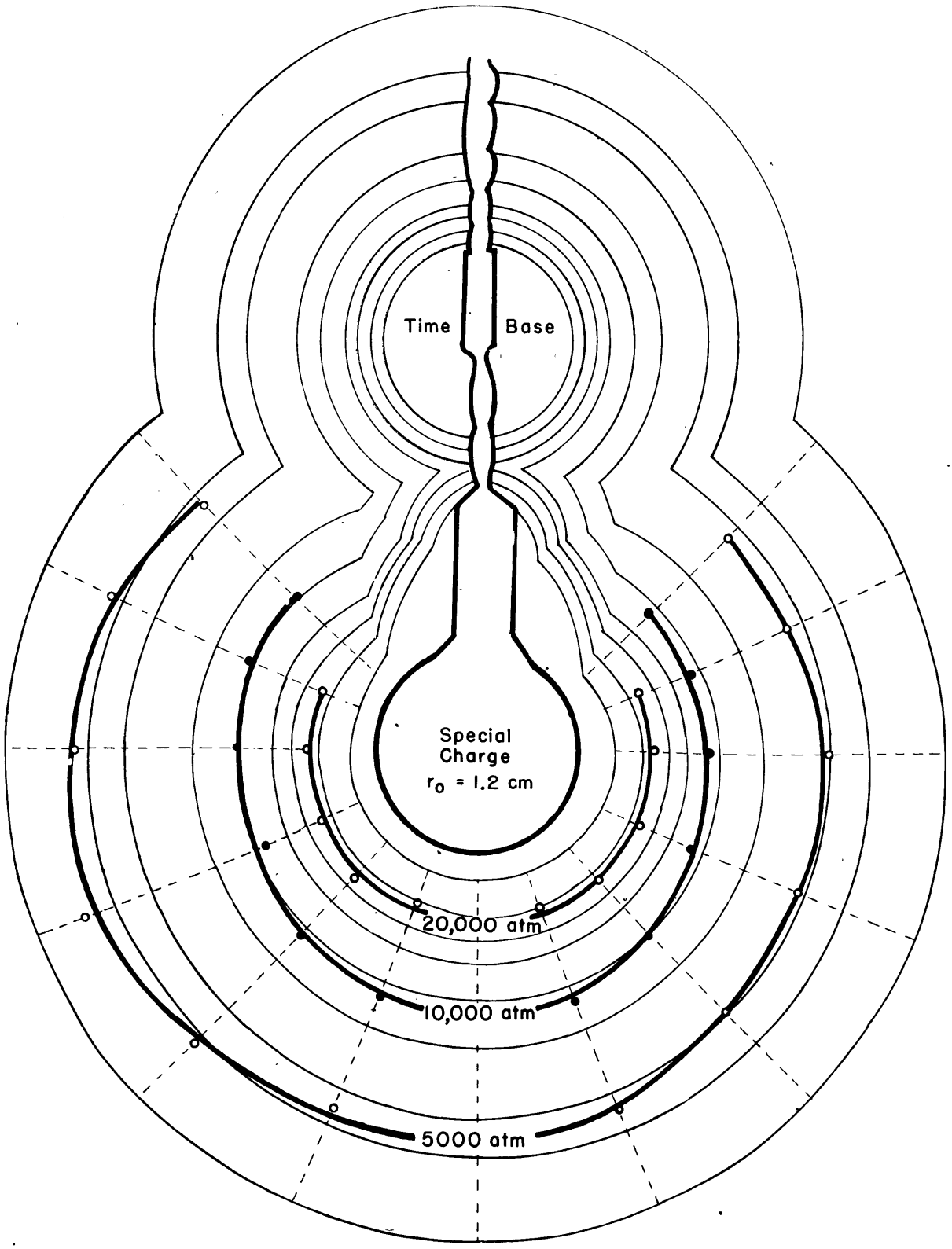

Figure 7 - Propagation of a Nearly Spherical Shock Wave

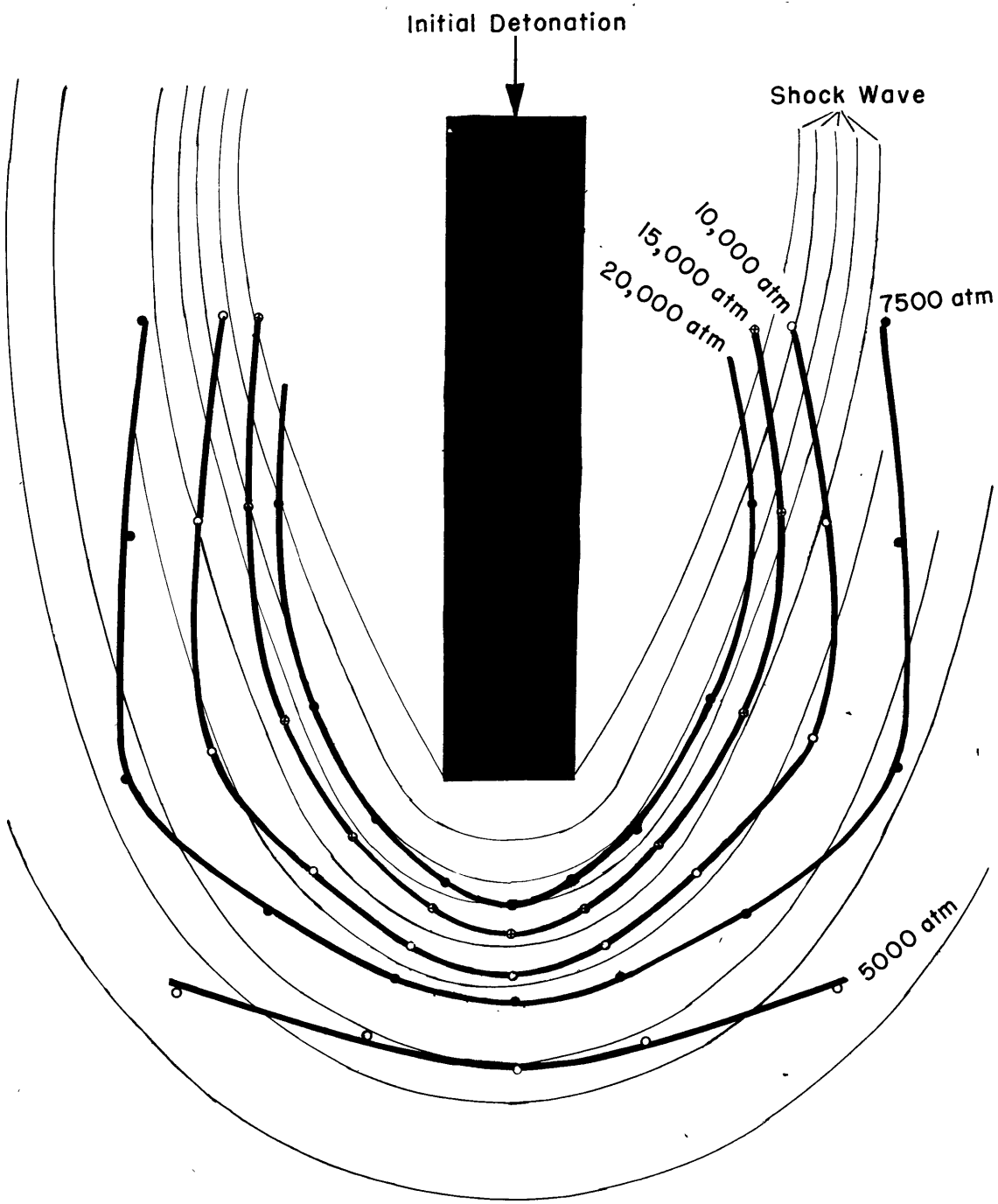

Figure 8 - Example of Propagation of a Nonspherical Shock Wave

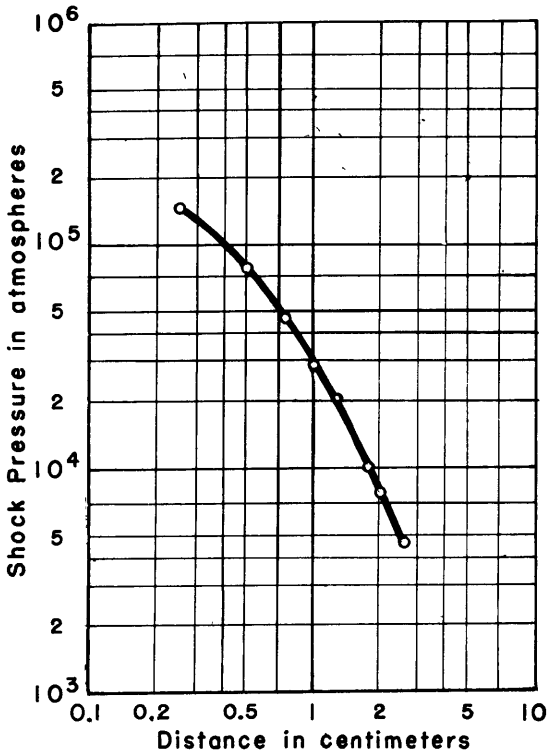

Figure 9 - Pressure Decrease with Distance from the End of the Line Charge (see Figure 8)

This charge, 12 mm in diameter, was fired from one end.* While the reaction of the explosive progresses at a velocity of 7750 meters per second, the shock wave generated at every point on the interface propagates and thus gives rise to the wave fronts plotted in Figure 8. For purposes of analysis, the pressure drop was determined in eleven different directions by means of the distance-time curves, and then a few constant-pressure curves were plotted.

In addition, a special analysis was made to find the values of the shock wave in the direction of the wave of detonation, for these values are of particular interest. This was accomplished by measuring several original photographs directly, and showed a drop in pressure as plotted in Figure 9. By extrapolation to the surface of the explosive, pressures are found for the transition of the wave of detonation into the surrounding medium, i.e., into the water, which are above 10 atmospheres. This agrees well with the expected order of magnitude of 10 atmospheres for the detonation wave; compare Reference (6).

SUPERPOSITION OF SHOCK WAVES

The difference of the behavior of shock waves from that of ordinary sound waves is particularly evident in superposition of two such waves. For sound waves, the pressures merely add according to the familiar principle of undisturbed superposition. This is valid on the basis of the equation for these waves, linearized with the aid of the simplifying assumption of infinitely small amplitude. Likewise, the velocity of propagation is not a function of the amplitude. For shock waves, on the other hand, the wave equation is not linear and the velocity of propagation becomes a function of the amplitude; see Figure 4.

---

* Doubts that such thin line charges detonate normally are not justified. Analysis showed that combustion proceeded at the same velocity as in ordinary line charges of 20 mm diameter.

The new phenomenon produced by superposition of shock waves was first noted by Mach (2) and is therefore termed Mach's angle or also Mach's V-propagation. Mach observed it when he detonated two small heaps of mercury fulminate simultaneously on a plate coated with soot. He got the results shown in Figure 10. Disregarding the two circles A and B about the point of detonation, where the soot was left in place owing to peculiarities of the experimental apparatus described in Reference (2), a sharp line can be seen in the center between the two points where the soot was also left in place. This line divides upward or downward sooner or later depending upon the intensity of the explosion and the consequent intensity of the shock wave, so that a V-shaped figure is produced in each case. It is to this phenomenon that the effect owes its name.

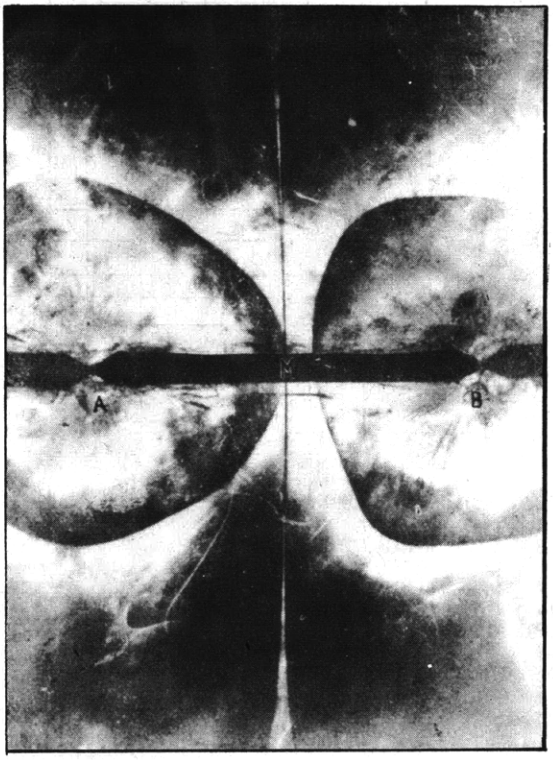

Figure 10 - Mach's V-Propagation in Air (According to C. Cranz and H. Schardin)

Now, it is known that the profile of shock waves is much less regularly developed in air than in water, in which the wave front is quite smooth. On the other hand, the velocity of a shock wave is far more a function of the amplitude in air than in water. Therefore the Mach V-effect in water, to be investigated in the following, is more difficult to observe but is more uniform and better for purposes of study.

Before taking up details, the explanation of the phenomenon will be given. The shock waves emanating from A and B intersect at points C and D as sketched in the accompanying figure. For superposition of normal waves the pressure at C and D is twice that for simple waves. However, conditions are more complex for shock waves, so that it can be stated only that the pressure P' at the point of intersection is higher than the pressure P of the individual wave.

Hence the compression impulse, proceeding from these points of intersection in the direction indicated by the arrows, propagates at a velocity a' which is greater than the velocity a of both the superposed waves.

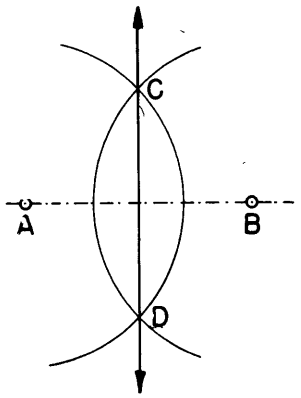

Now the points of intersection C and D move at the velocity

$$u = \frac{a}{\sin\alpha} > a$$

The value of u is very great in the vicinity of the line connecting the two charges and decreases with distance from this line. However, the value of u always remains greater than a. Also since a' is greater than a, from a given distance onward u may become less than a'. Then a compression impulse is released from the point of intersection and runs ahead of the latter point. In Mach's experiments on the glass plates coated with soot, which have been cited previously, this shock wave blew the soot away and thus produced the V.

The correctness of this explanation of Mach's V-propagation has been confirmed by investigations made by Cranz and Schardin (2). For superposition of ordinary sonic waves $a' = a < u$, and therefore a compression impulse can never be released to propagate as outlined previously.

This effect in water was observed for the first time during measurements of the pressure field about explosive charges of various shapes and about explosive charges variously detonated. Whereas the pressure field shown in Figure 9 was produced by initiating detonation of a length of explosive at one extremity, the entirely dissimilar conditions shown in Figure 11 result from initiating detonation at both ends of the stick of explosive simultaneously. For greater clearness again a segment only is given of the propagation pattern recorded by the high-speed spark camera. To further improve the clarity of the picture, moreover, such unessentials as the firing leads and even the linear scale and time calibration marks have been omitted.

In this propagation scheme, it is interesting to note that the wave fronts first separated off, numbered 1 and 2, continue to superpose undisturbed only in wave front 3. The succeeding wave fronts 3 to 9 show distinctly that the primary points of intersection of the two first waves become increasingly equalized. The superposition wave meets the first two wave fronts with a distinct break. The broken lines sketched into Figure 11 connecting these breaks in the wave fronts form a sort of V, which is a visual indication of the presence of a V-effect. The two shock waves superposed on each other, however, are interconnected in a manner making it difficult to check and to distinguish them from each other because they were produced by detonation along the same stick of explosive.

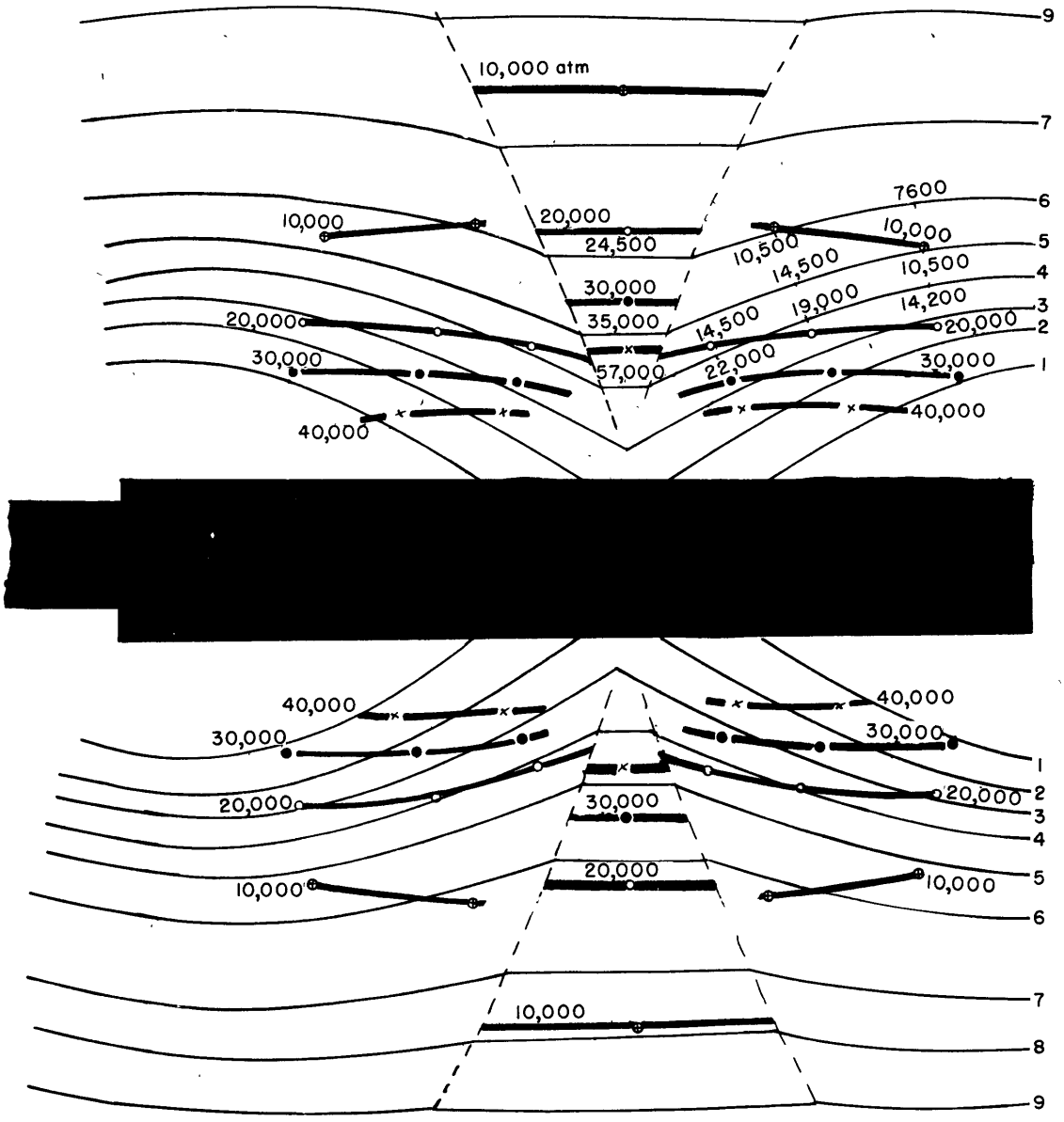

Figure 11 - Superposition of Two Shock Waves

The evaluation of the propagation pattern produced the constant-pressure curves plotted in Figure 11. The pressure values given along wave fronts 4, 5, and 6 are clearer. They show that the pressure in the superposition wave is higher than twice the shock-wave pressure.

The disadvantage inherent in the foregoing experimental arrangement, namely the production of both shock waves by the same charge, was obviated by the setup used for the subsequent propagation chart shown in Figure 12. In this figure again only the section of interest of the actual image field was reproduced, and the linear scale, time calibration, and firing leads were

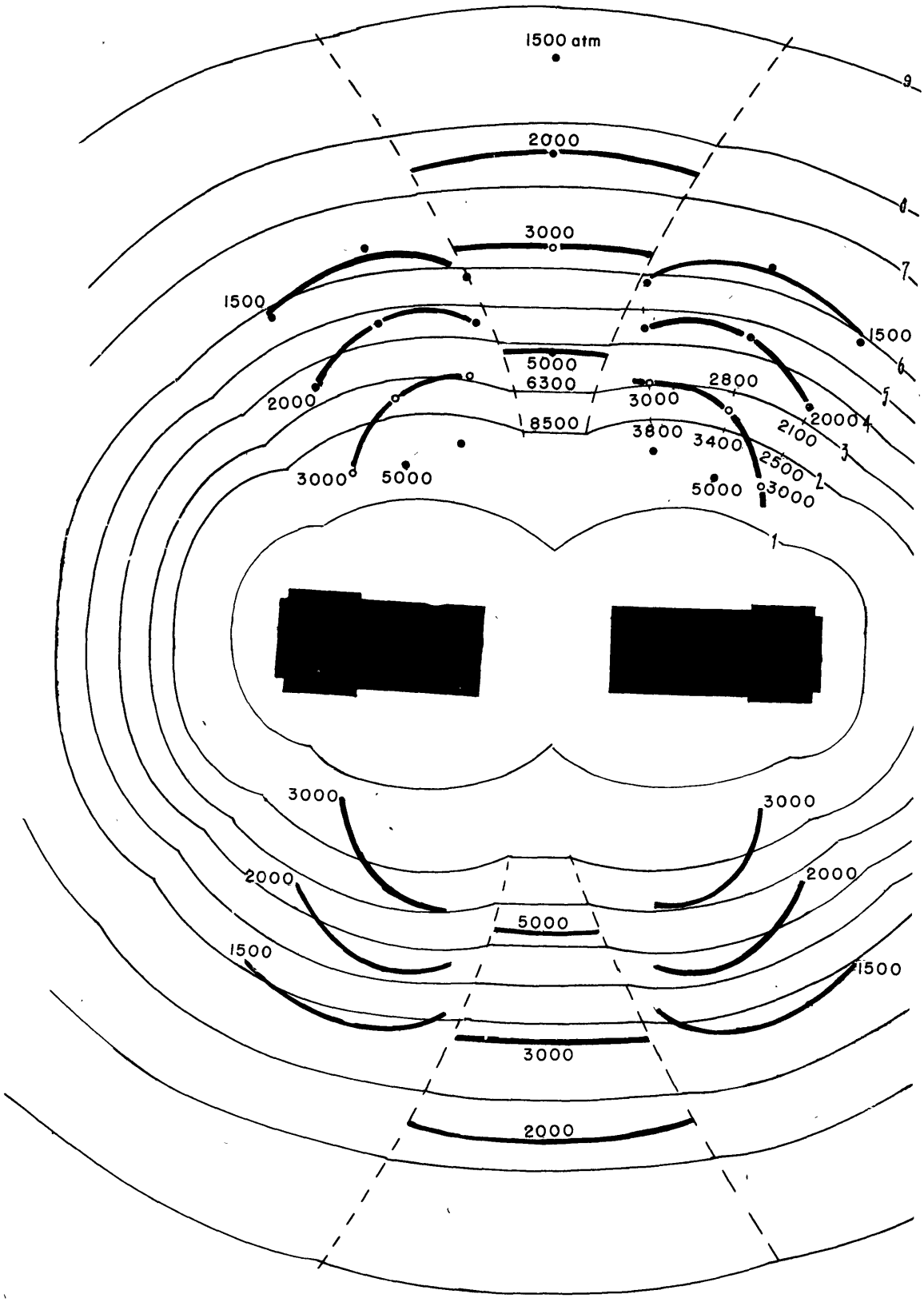

Figure 12 - Superposition of Two Separately Produced Shock Waves of Nearly Spherical Form

omitted. To produce two shock waves, two detonators, each consisting of 0.2 gm of lead azide and 1.4 gm of PETN were electrically set off simultaneously. The wave fronts are numbered 1 to 9.

Whereas the first front 1 still shows the normal point of superposition, from wave front 2 on the superposition wave is present, which becomes a clearly evident break in the two primary wave fronts. It is responsible for producing the effect that at more remote distances from the center of detonation the contour of the wave front is approximately spherical.

The constant-pressure curves drawn in likewise show, just as clearly as the curve of the wave front does, that there was no precisely spherical original wave. Despite this, however, it can be recognized that the amplitude of the superposition wave was again greater than twice the pressure of the shock wave. The numerical values for the pressures included for wave fronts 2 and 3 indicate this also.

For increasing the pressure in the superposition wave above the sum of the two superposed waves, the analysis plotted in Figure 13 is significant. In that figure the pressure drop of the superposition wave is plotted as a function of the distance from the axis of the charge for the test arrangement given in Figure 12. Moreover, the data are given for three different distances between the two detonators. The curve pertaining to zero distance, i.e., detonators in contact, is designated by I, the curves for distances of 1.5 cm and 3 cm are marked by II and III respectively. In the foregoing, it should be noted that, even in the case where the detonators are touching, two shock waves are produced as the detonators were fired separately. It can be recognized that within the ranges here considered the intensity of the superposition wave increases with the distance between the charges.

DISTURBED PRESSURE ZONES

With the foregoing method for the measurement of pressure fields, which has been applied to several examples, another problem can be attacked. In the following this problem will be taken up. The photographs, taken by O. von Schmidt (10), of the propagation of shock waves in the vicinity of the boundary layer between two media led to the discovery of a wedge-shaped wave front which was interpreted as so-called "head wave" by this scientist. Stimulated by these investigations, Joos and Teltow (11) showed that this wave front is explicable by the general formulas for wave propagation and that this result in principle had already been treated in a study by Sommerfeld (12) on the propagation of electromagnetic waves along the surface of the earth. However, these studies only treat the case in the vicinity of the boundary layer with the additional assumption that the primary spherical

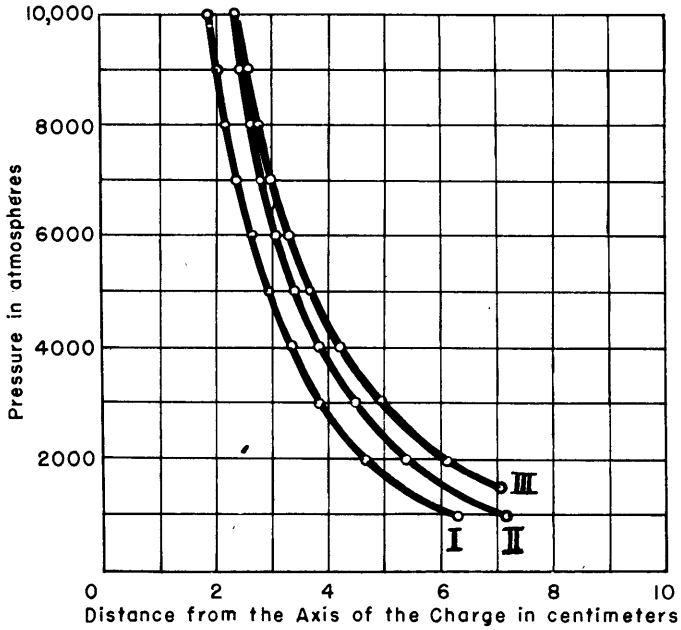

Figure 13 - Decrease of the Pressure with the Distance for Two Superposed Shock Waves

The test setup is shown in Figure 12. The distance between the detonators was 0 cm for I, 1.5 cm for II, and 3 cm for III.

wave is produced in the boundary layer. More exhaustive investigations of the problem as a whole by H. Ott (13) and particularly by M. Krüger (14), who accomplished the general theoretical treatment of the problem, furnish not only data for the various wave fronts but, in addition, exact data respecting the intensities occurring in them.

The theoretical treatments of the problem given previously were all made for the case of electromagnetic waves, but can be converted in a relatively simple manner to acoustic conditions, as already done by Joos and Teltow (11). By traversing the boundary to great distances, the spherical and conical waves, or wedge-shaped waves, become plane waves. In the formulation by Joos and Teltow, then, the following is found:

In the more rarefied medium, a nonhomogeneous plane wave propagates at the phase velocity ω/k_1 of this medium, parallel to the boundary layer. The planes of equal phase are perpendicular to the boundary layer. The amplitude is the combination of a constant component and a component deflected in phase by 90 degrees. The latter component increases in ratio to the height z, but naturally not to any arbitrary value, since z was assumed to be much less than r. Hence, this wave corresponds to the leading spherical wave in the rarer medium in O. von Schmidt's experiment. In the present approximation, this wave appears as a plane wave. The decrease of the amplitude toward the boundary layer can also be seen clearly on the schlieren photographs.

The conditions in the denser medium, i.e., in the hard sponge ebonite, are not of interest here, as the appertaining wave fronts cannot be traced owing to the opacity of the medium.

Although the photographs taken by O. von Schmidt had shown the peculiarities in the vicinity of the boundary layer, they permitted conclusions only respecting the wave fronts and not concerning the pertinent amplitudes - even though inferences can be drawn regarding them from the varying intensity of the refraction patterns.

Now, for the case of shock waves in the vicinity of a boundary layer, conditions are similar in principle and it is an obvious step to apply the method described previously herein for the measurement and plotting of pressure fields. Figure 14 shows such a propagation chart. The shock wave shown was produced in the boundary layer.

The testing arrangement used was as follows: In a sponge ebonite plate about 20 by 20 cm and approximately 2 cm thick a cylindrical explosive charge was set at the center. (Sponge ebonite is a synthetic plastic, made spongy by trapping a great number of small air bubbles. It has considerable mechanical strength but can be cut readily with a saw. Its specific gravity is about 0.1. At somewhat greater pressures, the ebonite framework of the structure collapses.) This hard sponge ebonite, which practically consists of air only, can be considered as an air space for the extremely intense shock waves here involved.

The propagation chart given in Figure 14 shows the development of the shock wave. The spherical wave used as a time calibration is barely indicated, to avoid disturbing the picture as a whole. In the lower portion of the picture a linear scale graduated in centimeters can be seen.

In the vicinity of the boundary layer the individual shock-wave fronts show a pronounced distortion. This is apparently to be interpreted to signify that the shock wave produced in the sponge ebonite at first propagates at greater velocity as a shock wave in air than subsequently in water. (The propagation of such waves occurs at first at practically the velocity of detonation and then very quickly drops to sonic velocity in air.) This shock wave running ahead of the wave in water must draw a "head wave" in its wake, as the propagation chart actually reveals and confirms. Not until greater distances from the explosion have been traversed does the value of the shock wave propagating in the sponge ebonite drop below the value of the shock wave traveling in water, which is still propagating at supersonic speed. Somewhat later, therefore, the shock wave in water runs ahead and it alone remains visible.

This condition occurred for the three outer shock-wave fronts sketched in. It is here revealed that the wave surface which originally was uniformly curved bends in the direction of the boundary layer and lags. This is apparently to be explained as the result of expansion (pressure release) in the readily destructible spongy structure of the sponge ebonite. However, as a result and on the basis of the relationship between pressure and velocity for a shock wave as given in Figure 4, the velocity of propagation of these portions of the shock wave must decrease. Hence a lag of the wave front is produced in that region.

The constant-pressure curves plotted together in the propagation chart shown in Figure 14 reveal this flattening of the shock wave in water as contrasted with air somewhat more clearly. Even if the curve of the individual isobars was initially somewhat distorted by the shape of the explosive charge, especially the curves for 10,000 and 5000 atmospheres, the downward deflection of the curve for 2000 atmospheres still shows that the effect occurred.

It should be pointed out here that this pressure drop toward the boundary layer naturally occurs for normal sonic vibrations also. However, it can only be distinguished directly at the wave front on shock waves, as only in the case of such waves of great amplitude does the velocity of propagation become a function of the amplitude.

A clearer picture of conditions is obtained by eliminating the disturbances described in the foregoing. Here the charge was a short distance away from the narrow side of the plate of sponge ebonite so that a nearly spherical shock wave in water at an initial pressure of 3000 atmospheres passes over the plate. The fronts of the shock wave before arrival at the plate (Numbers 1 and 2, Figure 15) have a uniform curvature which has not yet begun to change shortly after the wave front has reached the plate (Number 3). The subsequent wave fronts, from 4 on, however, deflect toward the boundary layer with constantly increasing curvature, lagging as they do. A possible explanation has already been given.

The plotting of the propagation chart was performed along eight trajectories, to determine the pressure. The isobars shown in Figure 15 were obtained. They reveal how the undisturbed wave which was practically spherical originally is later flattened in the direction of the boundary layer.

The present material is not sufficiently extensive to permit any more specific statements to be made respecting the pressure drop toward the

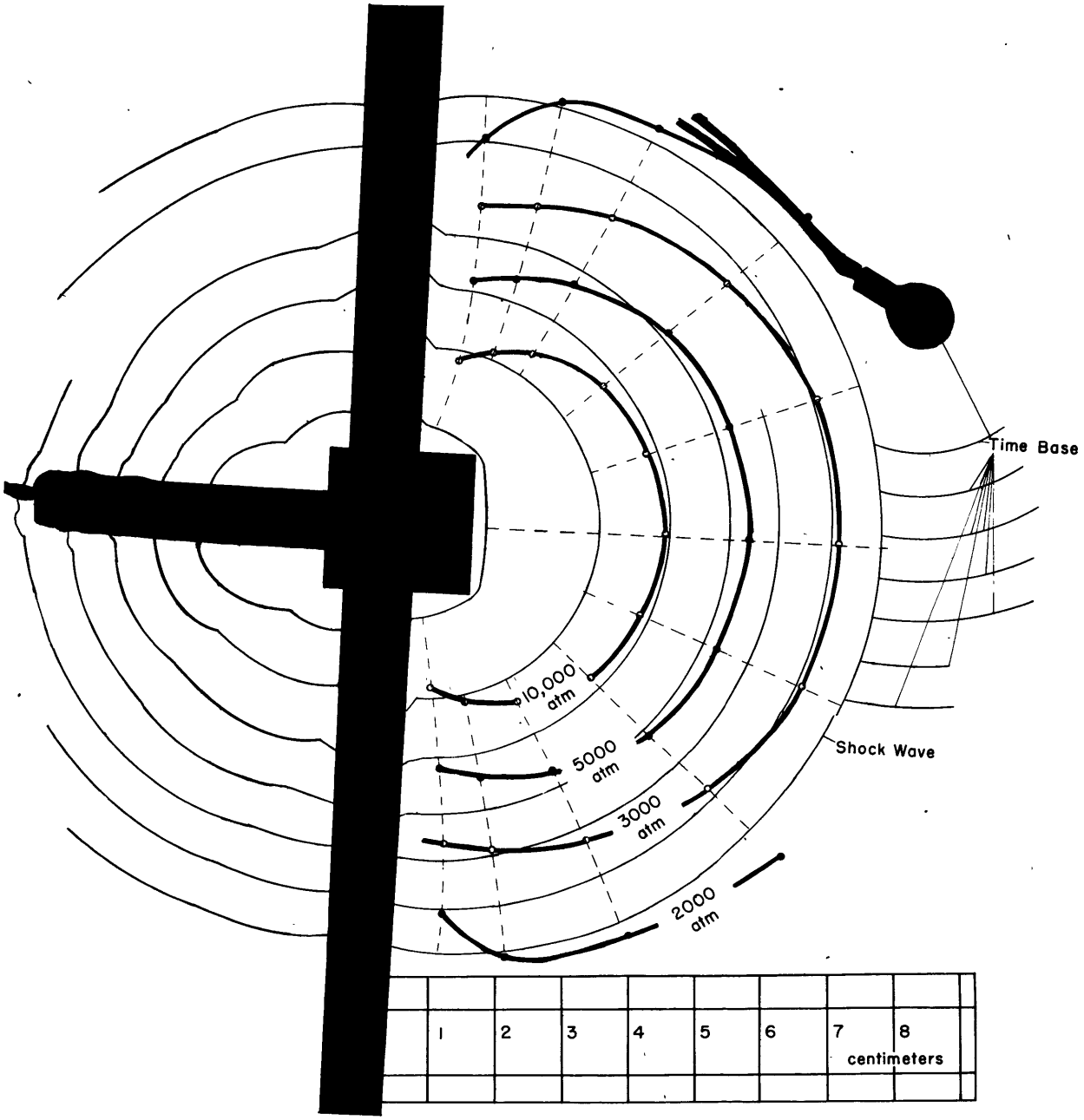

Figure 14 - Pressure Field of a Shock Wave Produced in a Boundary Layer

For an explanation of the time base, see page 7.

boundary layer. However, the two evaluations given clearly show the principal phenomena for shock waves in the vicinity of a boundary layer between water and air and the applicability of the method here outlined for the investigation of the problem.

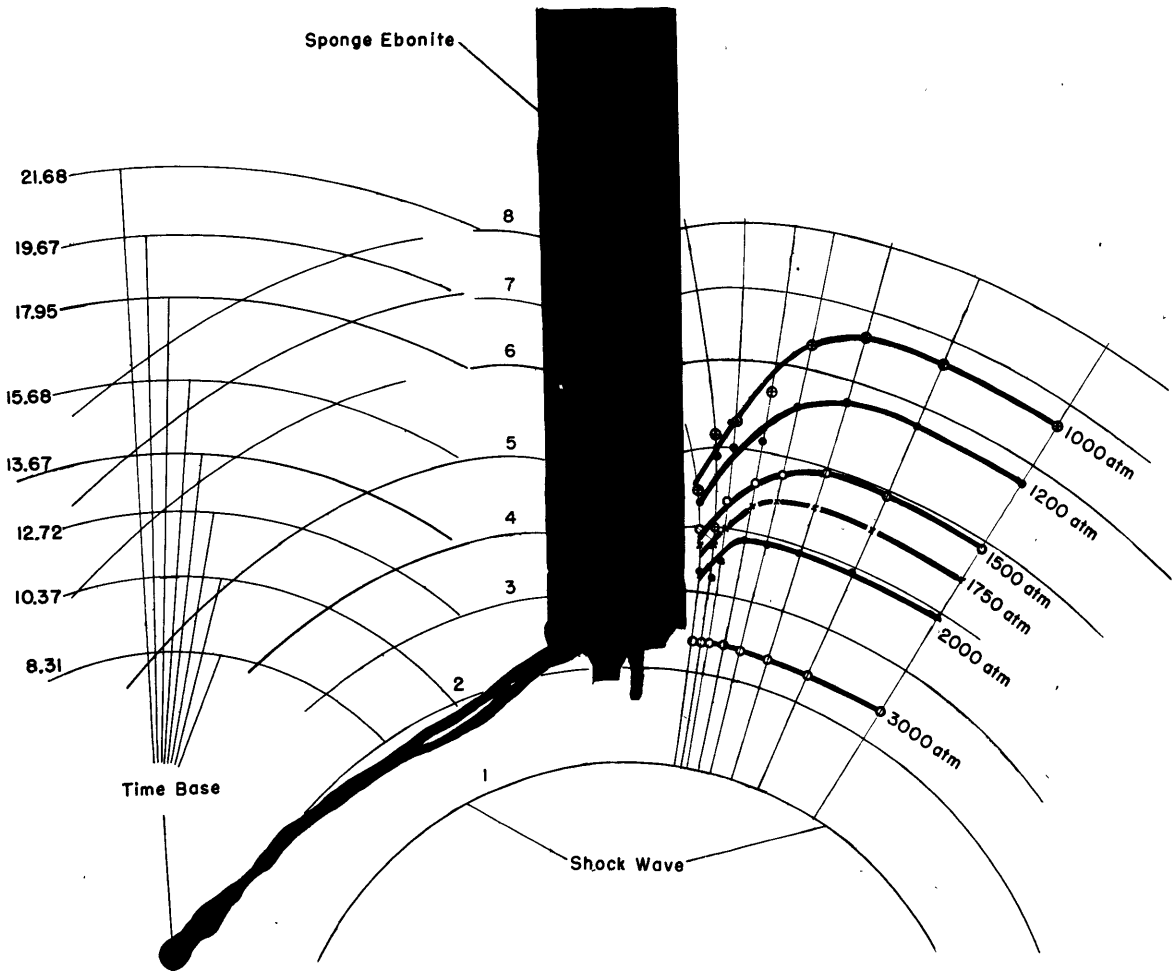

Figure 15 - Pressure Field Produced by a Shock Wave in the Vicinity of a Boundary Layer

SUMMARY

The velocity of intense shock waves is a function of their amplitude. The relationship can be derived for plane wave fronts from the general formulas for shock waves and also from the equation of state of the medium wherein the propagation occurs.

With the aid of the high-speed spark camera the propagation of the wave front of very intensive and hence of very high-speed shock waves can be recorded. The velocity of propagation can be determined from the distance-time curves recorded photographically by a high-speed spark camera. On the basis of the theoretical relationship mentioned above, the amplitudes of the shock wave can be determined from the foregoing.

Analysis of several orienting experiments shows that the method used in conjunction with the experimental apparatus described furnishes usable results and is particularly suitable for determination of the pressure fields of shock waves.

The high-speed spark photographs here used were taken at the former Chemisch-Physikalische Versuchsanstalt der Marine (Chemical-Physical Research Institute of the German Navy). My special gratitude is extended to Commander Springer of the U.S. Navy for making it possible to complete this study.

REFERENCES

(1) "Membrandruckdosen" (Diaphragm Pressure Gages), by A. Keil, CPVA Report, Kiel, 1945.

(2) "Kinematographie auf ruhendem Film und mit extrem hoher Bildfrequenz" (Cinematography on Stationary Film at Extremely High Image Frequency), by C. Cranz and H. Schardin, Zeitschrift für Physik, Vol. 56, 1929, pp. 147-183.

(3) "Die Schlierenverfahren und ihre Anwendung" (Schlieren Methods and their Use), by H. Schardin, Ergebnisse der exakten Naturwissenschaften, Vol. 20, 1942, pp. 303-439.

(4) J. Hermes, University of Bonn, Mathematical Treatise, unpublished.

(5) H. Hugoniot, Journal de l'Ecole Polytechnique, Paris, 1887-1889.

(6) R. Becker, Zeitschrift für Physik, Vol. 8, 1922, p. 321 et seq.

(7) "Verhalten von Wasser als Flüssigkeit und in 5 festen Formen unter Druck" (Behavior of Water as a Liquid and in 5 Solid Forms under Pressure), by P.W. Bridgman, Proceedings of the American Academy of Arts and Sciences, Vol. 47, 1912, pp. 441-558. Also cited in Zeitschrift für Anorg. Chemie, Vol. 77, 1912, p. 377 et seq.

(8) "Zustandsgleichung für Wasser bei sehr hohen Drucken und die Geschwindigkeit einer Stosswelle in Wasser" (Equation of State for Water under High Pressure and the Velocity of a Shock Wave in Water), by G. Burkhardt, Ballistische Institut, Gatow, 1942.

(9) W. Döring, University of Göttingen, assumed to be unpublished.

(10) O. von Schmidt, Physikalische Zeitschrift, Vol. 39, 1938, p. 868.

(11) G. Joos and J. Teltow, Physikalische Zeitschrift, Vol. 40, 1939, p. 289.

(12) A. Sommerfeld, Annalen der Physik, Vol. 28, 1909, p. 665.

(13) H. Ott, Annalen der Physik, Vol. 41, 1942, p. 443.

(14) M. Krüger, Zeitschrift für Physik, Vol. 121, 1943, p. 377.